

In Situ Imaging of Tissue Remodeling with Collagen Hybridizing Peptides

Jeongmin Hwang,^{†,||} Yufeng Huang,[‡] Timothy J. Burwell,[§] Norman C. Peterson,[§] Jane Connor,[§] Stephen J. Weiss,[⊥] S. Michael Yu,^{†,‡,||} and Yang Li^{*,†,||}

[†]Department of Bioengineering and [#]Department of Pharmaceutics and Pharmaceutical Chemistry, University of Utah, Salt Lake City, Utah 84112, United States

^{||}3Helix Inc, Salt Lake City, Utah 84117, United States

[‡]Division of Nephrology and Hypertension, Department of Internal Medicine, University of Utah School of Medicine, Salt Lake City, Utah 84132, United States

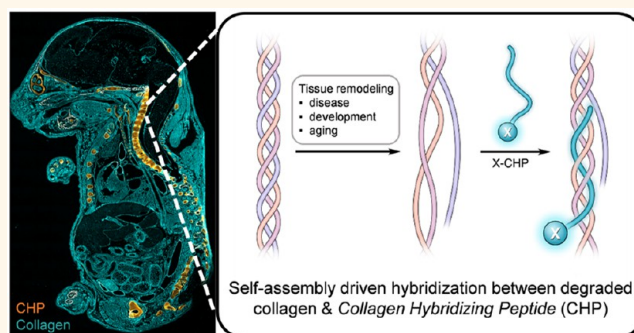
[§]MedImmune LLC, Gaithersburg, Maryland 20878, United States

[⊥]Division of Molecular Medicine & Genetics, Department of Internal Medicine, and the Life Sciences Institute, University of Michigan, Ann Arbor, Michigan 48109, United States

Supporting Information

ABSTRACT: Collagen, the major structural component of nearly all mammalian tissues, undergoes extensive proteolytic remodeling during developmental states and a variety of life-threatening diseases such as cancer, myocardial infarction, and fibrosis. While degraded collagen could be an important marker of tissue damage, it is difficult to detect and target using conventional tools. Here, we show that a designed peptide (collagen hybridizing peptide: CHP), which specifically hybridizes to the degraded, unfolded collagen chains, can be used to image degraded collagen and inform tissue remodeling activity in various tissues: labeled with 5-carboxyfluorescein and biotin, CHPs enabled direct localization and quantification of collagen degradation in isolated tissues within pathologic states ranging from osteoarthritis and myocardial infarction to glomerulonephritis and pulmonary fibrosis, as well as in normal tissues during developmental programs associated with embryonic bone formation and skin aging. The results indicate the general correlation between the level of collagen remodeling and the amount of denatured collagen in tissue and show that the CHP probes can be used across species and collagen types, providing a versatile tool for not only pathology and developmental biology research but also histology-based disease diagnosis, staging, and therapeutic screening. This study lays the foundation for further testing CHP as a targeting moiety for theranostic delivery in various animal models.

KEYWORDS: matrix metalloproteinase, triple helix, fibrosis, inflammation, bone formation, targeted delivery



Collagen is the major structural component of the extracellular matrix (ECM) present in virtually all mammalian tissue and organs,¹ with an essential role in supporting cell attachment, proliferation, migration, and differentiation.^{1,2} While collagen synthesis and degradation are delicately coordinated during tissue development and homeostasis, excessive collagen remodeling has also been implicated in numerous pathologic states.^{3–5} For example, collagen degradation mediated by matrix metalloproteinases (MMPs) is responsible for cancer progression and metastasis.^{6–8} In atherosclerosis, the thinning and weakening of the fibrous collagen cap by enzymatic degradation renders atherosclerotic plaques susceptible to rupture, resulting in myocardial infarction and sudden cardiac death.⁹ Likewise, the

degeneration of type II collagen, the predominant structural protein in cartilage, is a key pathogenic step in osteoarthritis.^{10,11} Independent of its pathologic roles, orchestrated remodeling of the collagen matrix is also crucial in many developmental events, such as bone formation and mammary gland morphogenesis.⁴ Therefore, imaging techniques that detect proteolyzed collagen in isolated tissues would provide a powerful tool for assessing the tissue remodeling states associated with a variety of developmental or pathologic

Received: May 6, 2017

Accepted: September 6, 2017

Published: September 6, 2017

events; a molecular agent that targets the degraded collagen would also enable site-specific delivery of theranostic molecules for medical applications.

Despite the obvious importance of collagen remodeling, current collagen-targeting and imaging tools either cannot detect degraded collagen or have significant limitations. For example, widely used collagen stains, such as Masson's trichrome or Picrosirius red, rely purely on electrostatic interactions for binding¹² and cannot distinguish intact collagen from the degraded.¹³ Likewise, most anticollagen antibodies are made for multiple applications under both denaturing and nondenaturing conditions (e.g., in Western blot and immunohistochemistry), indicating that their affinities are not affected by the collagen conformation. Antibodies with higher specificity have been developed to recognize degraded collagen as a consequence of the generation of new N- or C-terminal epitopes or as soluble collagen fragments, but only for a handful of the 28 mammalian collagen subtypes.^{14–19} More importantly, these antibodies fail to detect collagen fragments in tissues if specific epitopes are lost following more extensive proteolysis. Microscopic methods, such as second-harmonic generation (SHG) and transmission electron microscopy (TEM), have also been used to visualize fibrillar collagen²⁰ where a reduction of SHG signal²¹ or the disruption of the periodic D-banding pattern in TEM^{22,23} can indicate alteration of collagen structure. However, such measurements are based on the loss of signal or structural features at the fiber scale that does not directly reveal the degradation events occurring at the molecular level.

We envisioned that the triple-helical structure of collagen provides a unique mechanism for targeting collagen degradation.^{24,25} All of the 28 collagen subtypes found in mammals share a basic structural motif in which the three protein strands intertwine into a triple helix stabilized by interstrand hydrogen bonds (Figure 1).² Importantly, this supersecondary con-

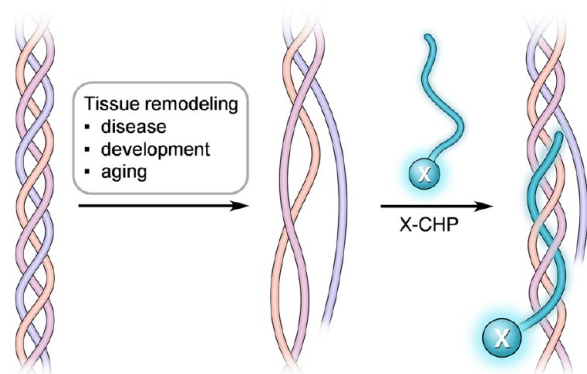


Figure 1. Schematic of a CHP strand (labeled with X) hybridizing to denatured collagen chains and forming a collagen triple helix. During disease progression, tissue development, or aging, collagen can be extensively degraded by collagenolytic proteases, causing its triple helix to unfold at the physiological temperature due to reduced thermal stability. X represents the biotin or fluorescent tag.

formation is nearly exclusive to collagens.²⁶ Nevertheless, following degradation by collagenolytic proteases, such as those belonging to the matrix metalloproteinase or cysteine proteinase families, the fragmented collagen triple helices are no longer thermally stable at body temperature and spontaneously unfold (Figure 1), leaving the denatured

collagen fragments covalently cross-linked within the partially degraded, insoluble collagen matrix.^{24,27–29} To unequivocally detect proteolyzed collagen *in situ*, we set out to develop a synthetic peptide termed the collagen hybridizing peptide (CHP), which specifically binds to denatured collagen strands by re-forming a triple-helical structure in a fashion that is similar to primer binding to melted DNA strands during polymerase chain reactions (PCRs) (Figure 1).^{24,25,30,31} The CHP has a repeating sequence of glycine(G)–proline(P)–hydroxyproline(O), an amino acid triplet with the highest folding propensity for the triple-helical structure found among all GXY units in the native collagen sequence.³² The single-strand CHPs showed excellent ability to hybridize with unfolded collagen chains denatured by heat or protease activities,^{24,25,30,31,33,34} but negligible affinity to intact collagen due to the absence of binding sites. In addition, the neutral and hydrophilic amino acid composition of CHP makes it virtually nonadherent to other biomolecules.^{24,25}

In our previous work,^{24,25} we reported CHP's ability to target collagen remodeling caused by cancer xenografts and Marfan's syndrome *in vivo*. However, its ability to detect degraded collagen in isolated histopathologic samples has never been demonstrated. More importantly, it remained to be shown that the presence of degraded collagen is a hallmark feature shared by almost every tissue type and numerous pathologic conditions beyond cancer and Marfan's syndrome.^{3–5} In this study, we used fluorescence microscopy to evaluate the binding of CHPs labeled with 5-carboxyfluorescein (5-FAM) or biotin on a series of animal and human tissue samples that have undergone remodeling during representative pathologic (e.g., osteoarthritis, myocardial infarction, glomerulonephritis, lung fibrosis) and physiologic events (e.g., bone development, skin aging). We demonstrate that the CHP binding effectively reports the level and location of denatured collagen products generated *in vivo*. Given the wide distribution of collagen in mammalian tissues,¹ our results suggest that CHP represents a versatile, but simple staining tool for monitoring many, if not all, remodeling events in isolated tissues and a potential delivery vehicle for targeting a wide range of tissues damaged by disease or injury.

RESULTS AND DISCUSSION

Design of the Study. We selected the following tissue samples to investigate the specifics of CHP binding because they represent a full spectrum of known scenarios involving ECM remodeling and collagen degradation,³ ranging from tissue degeneration (e.g., osteoarthritis), acute inflammation (e.g., myocardial infarction), and fibrotic remodeling (e.g., glomerulonephritis and pulmonary fibrosis) to tissue development (e.g., embryonic bone formation) and aging (e.g., chronological skin aging).

Prior to staining pathologic tissues with CHPs, we evaluated and optimized the staining protocol using a set of ligament cryosections that had been heated to 80 °C to purposefully denature collagen. CHP was synthesized by solid phase peptide synthesis, followed by N-terminal labeling with either 5-FAM (designated as F-CHP) for fluorescence imaging or biotin (designated as B-CHP) for neutravidin/streptavidin-mediated detection *via* non-green fluorescence channels (e.g., Alexa-Fluor647-labeled streptavidin) or colorimetric reaction (e.g., horseradish peroxidase conjugated neutravidin). Because the CHP strands can slowly self-assemble into triple helices, thereby lose the driving force to hybridize with collagen, a

heating-and-quenching step was applied to the CHP solution immediately prior to staining (Figure S1, see Methods for details). Following this protocol, we detected strong fluorescence signals from F-CHP bound to heat-denatured ligaments in a concentration-dependent fashion using 1 to 100 μM of CHP (Figure S2A). We also observed that the fluorescence signal of F-CHP rises steadily as the staining time increases (Figure S2B). Based on these preliminary results, an optimal combination of CHP concentration (15–30 μM) and staining time (≥ 16 h) was used in subsequent experiments with native tissues.

Osteoarthritis. Type II collagen is the predominant component of cartilage, and its enzymatic breakdown represents a crucial molecular event during osteoarthritis (OA).^{10,11,35} As such, cryosections of human OA articular cartilage were stained with Safranin O and F-CHP, and tissue sites within the diseased region were compared to unaffected regions. Safranin O staining confirmed near intact architecture in normal regions of the cartilage tissue (Figure 2A). By

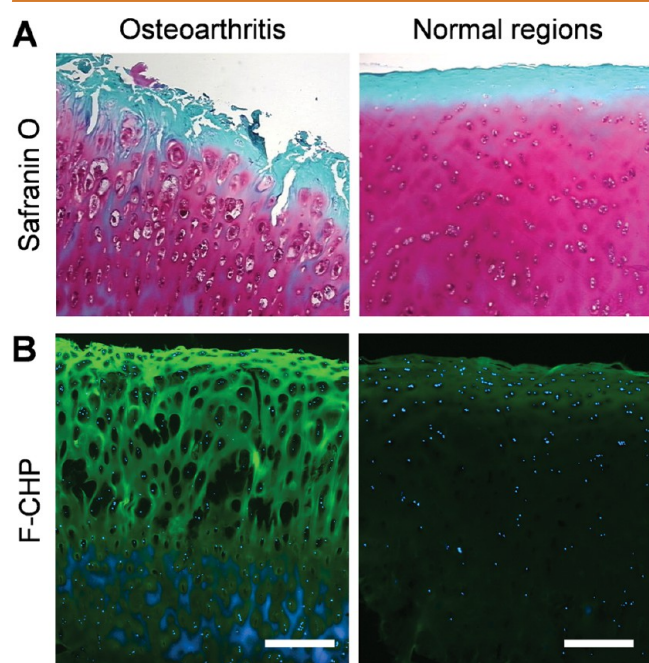


Figure 2. Osteoarthritis. Micrographs of articular cartilage tissue within the osteoarthritic or normal region from an OA patient. Sections from the same tissue samples were stained with Safranin O/fast green (A) or with F-CHP (B). Images of the Safranin O staining (A) were provided by the tissue supplier with permission (Copyright OriGene Technologies). In panel (B), Hoechst 33342-stained cell nuclei are shown in blue, and each image is representative of similar results from three stained sections. Scale bars: 500 μm .

contrast, in diseased regions, pathologic features of OA were clearly observed, including extensive vertical fissures and matrix fibrillation extending into the midzone, as well as enlarged lacunae and chondrocyte loss (Figure 2A). F-CHP staining highlighted fibrous structures with strong fluorescence intensity arising in the superficial and mid zones of the OA cartilage, indicating collagen degradation and denaturation (Figure 2B). Only low-intensity F-CHP fluorescence was observed in the superficial zone of the normal control (Figure 2B). Hence, our results confirm that matrices of normal and disease cartilage can be readily differentiated with CHP staining and that the

increased CHP binding to the OA tissue strongly suggests collagen degradation.

Myocardial Infarction. Following myocardial infarction (MI), degradation of the collagen matrix by the proteolytic enzymes released from infiltrating leukocytes is a major determinant of the irreversible tissue damage that occurs during the inflammatory phase of the disease process.³⁶ To visualize degraded collagen, cryosections of hearts harvested from mice at varying time points after occlusion of the left anterior descending artery³⁷ were probed with B-CHP and further visualized with AlexaFluor647-labeled streptavidin. Whole-heart fluorescence images demonstrate that denatured collagen is visible at day 3 post-MI, with the CHP signal increasing significantly at day 7 and persisting until day 14 (Figure 3A). F-CHP staining of sections from the same hearts alternately processed by paraffin-embedding showed similar results (Figure S3). The quantified CHP fluorescence signals obtained from whole-section scanning of the hearts within each group confirmed elevated levels of collagen degradation, which peaked at 1 week postinfarction (Figure 3B). This result is in agreement with previous studies on similar mouse models where MMPsense probes and zymography were used to demonstrate increased MMP activity that reached maximal levels at 1 to 2 weeks post-MI.³⁸ Interestingly, images of the 1-week post-MI hearts costained with B-CHP and an anti-CD68 antibody showed that the CHP binding was located in regions enriched with infiltrating macrophages (Figure 3, C and D), suggesting the correlation between collagen degradation and the recruited inflammatory cells.³⁶

Glomerulonephritis. Glomerulonephritis is a group of inflammatory kidney diseases characterized by glomerular damage.^{39–41} The destruction of glomerular architecture, in turn, accelerates remodeling of the surrounding extracellular matrix, thereby leading to fibrotic scarring (glomerulosclerosis).^{39–41} In the glomeruli of anti-Thy-1 nephritic rats, a classic animal model of glomerulonephritis, elevated MMP expression, and increased collagen deposition is well documented in the literature.^{40–43} As such, we first analyzed kidney cryosections harvested from the anti-Thy-1 nephritic and normal control rats with the conventional periodic acid–Schiff (PAS) stain. As expected, the amount of mesangial matrix occupying each glomerulus was higher in the affected kidneys (Figure 4A), confirming the fibrotic glomerular expansion. Following F-CHP staining, strong signals were recorded in the glomeruli of the nephritic animals with minimal staining intensity detected in normal kidneys (Figure 4B). Interestingly, the CHP signal is confined to the diseased glomeruli, whereas type IV collagen (visualized by immunofluorescence staining) is uniformly distributed in the tissue, including the interstitial space (Figure 4B). Similar results were obtained when the sections were stained with B-CHP and further visualized using horseradish peroxidase (HRP) conjugated neutravidin (Figure S4). Given that F-CHP signals and anti-collagen IV antibody staining were colocalized in the glomeruli (Figure 4B), the unfolded/degraded type IV collagen localized in the basement membrane region is the most likely target of CHP, though we cannot exclude the possibly of CHP binding to minor basement-membrane-associated collagen types.⁴⁴ Hence, the PAS and CHP staining results validate that nephritic glomeruli contain elevated amounts of collagen with a partially degraded and unfolded structure. The CHP stain pinpoints the glomerular lesion; such high specificity is nearly impossible to

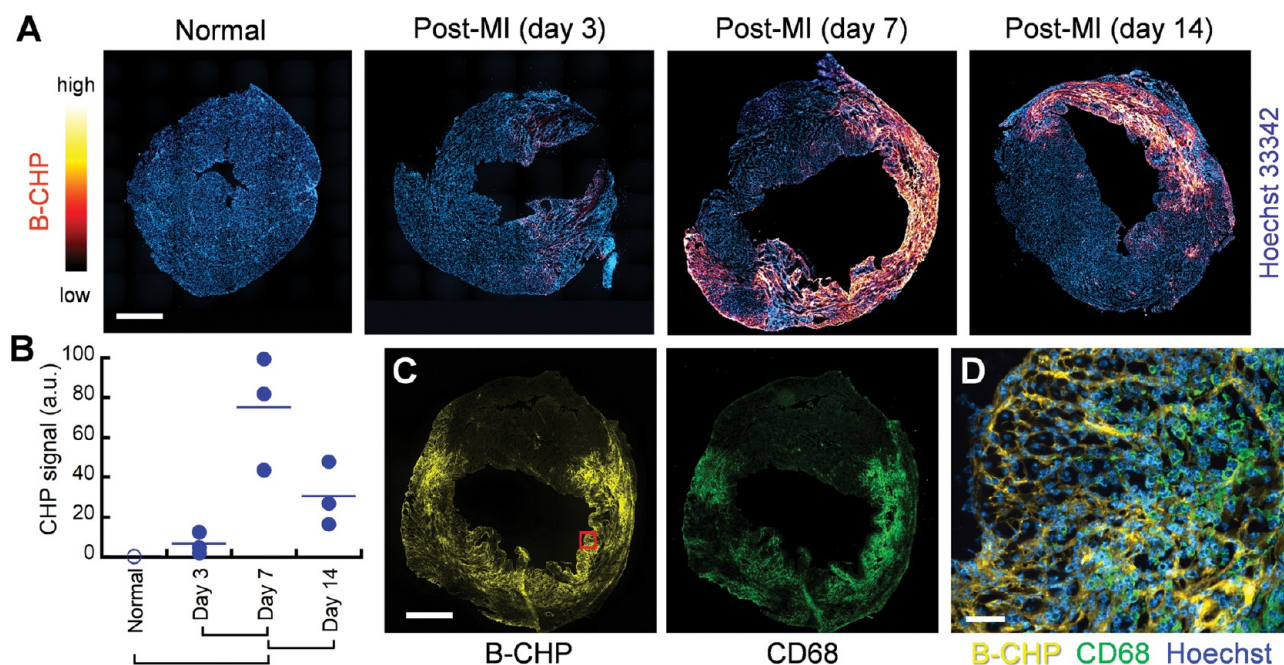


Figure 3. Myocardial infarction. (A) Representative fluorescence scans of axial cross sections of the mouse hearts before (normal) or at three time points after myocardial infarction (MI), stained with Hoechst 33342 (blue) and B-CHP (detected with AlexaFluor647-streptavidin, red-yellow). (B) Digitally quantified total CHP fluorescence signals in the whole-section scans of the three hearts in each group are shown (a.u. = arbitrary unit). The means of the paired groups labeled under the graph are significantly different (one-way ANOVA with *post hoc* Tukey HSD test, $P < 0.05$). (C) Fluorescence scans of a heart harvested 7 days after MI show close spatial similarity between signals from B-CHP and macrophages as detected with an anti-CD68 antibody. (D) A magnified view of the infarcted region within the red box in panel (C) with merged fluorescence signals shows that high level of degraded collagen is in areas crowded with macrophages. Scale bars: 1 mm (A, C), 50 μm (D).

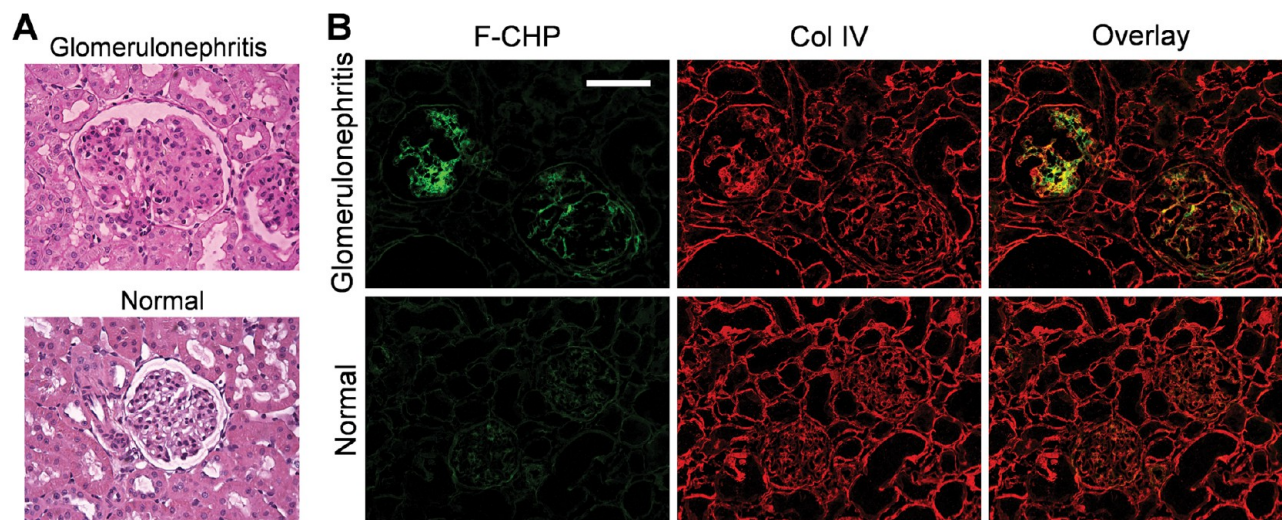


Figure 4. Glomerulonephritis. Representative micrographs of kidney cryosections from anti-Thy-1 nephritic and normal control rats stained with PAS (A) or F-CHP and an anti-collagen IV antibody (B). Images are representative of similar results from three animals within each group, three stained sections per animal. Scale bar: 100 μm .

achieve with conventional staining tools, which are typically insensitive to the structural change of their targets.

Pulmonary Fibrosis. Bleomycin is a chemotherapeutic agent with known pulmonary toxicity that leads to fibrotic changes in animal models that mimic those observed in idiopathic pulmonary fibrosis patients.⁴⁵ Aberrant wound healing responses, involving both increased MMP activity^{46,47} and excess matrix deposition,^{45,48} have been implicated in the pathogenesis of pulmonary fibrosis in this model. Using

MMPsense 680, a probe that fluoresces in the near-infrared region after MMP cleavage, we confirmed elevated MMP activity in the fibrotic lungs of bleomycin-treated mice relative to normal controls (Figure S5). To visualize the accumulation of damaged collagen within the remodeling lung matrix at the tissue and cellular levels, F-CHP staining was applied to a set of lung cryosections harvested at varying time points after bleomycin delivery *via* an implanted osmotic pump. F-CHP staining revealed the spotty distribution of damaged collagen,

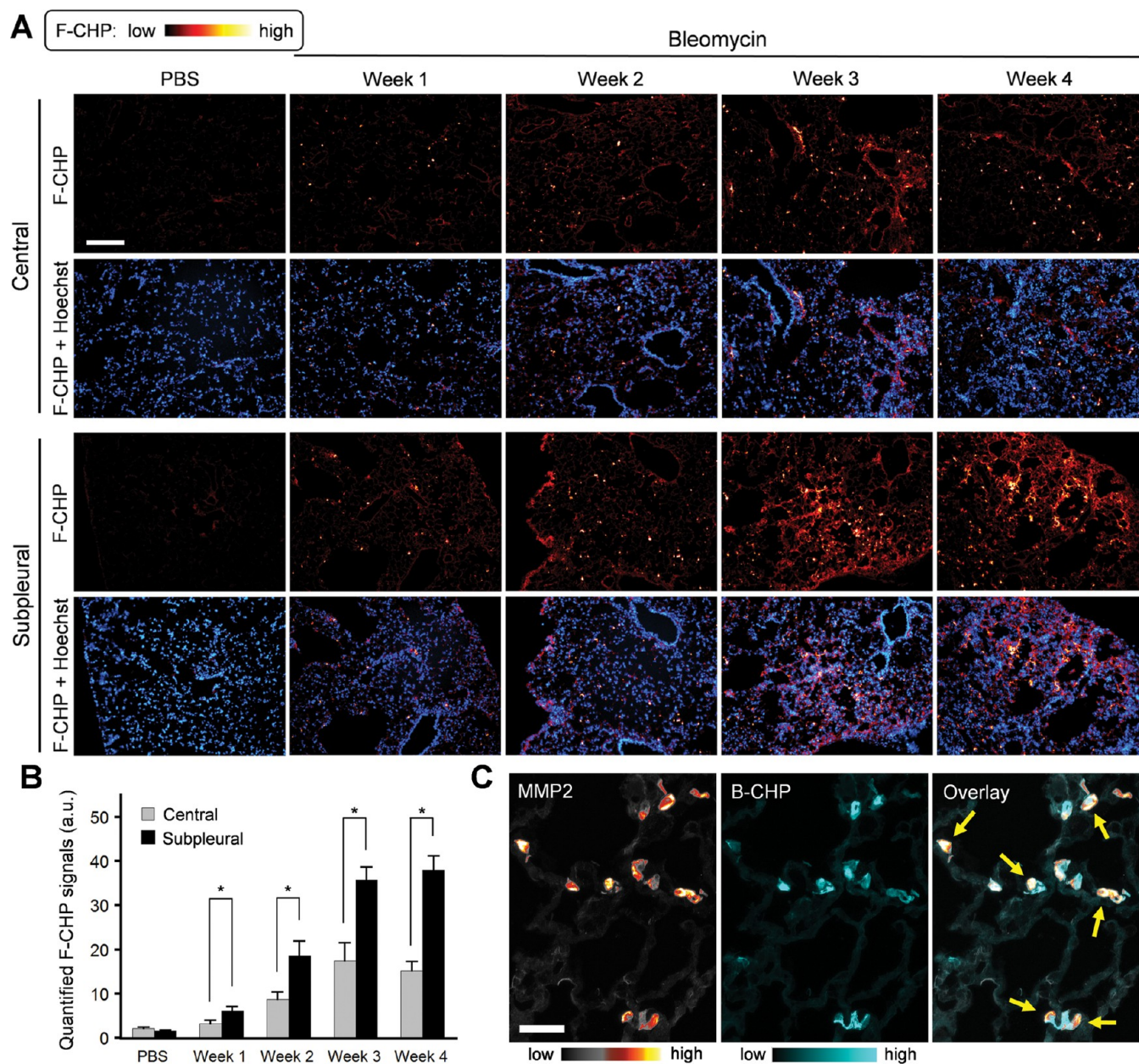


Figure 5. Pulmonary fibrosis. (A) Representative fluorescence micrographs of the central and subpleural areas of lung cryosections obtained from mice dosed with bleomycin through minipumps for varying time periods *versus* control mice dosed with PBS for 1 week, and stained with F-CHP and Hoechst 33342. Selected micrographs are representative of images collected from 3 animals per group. (B) Quantified signals showing the time course and spatial difference of F-CHP signal levels. Numbers are presented as the mean + standard error and analyzed using one-way ANOVA with *post hoc* Tukey HSD test. * indicates significant difference in means ($P < 0.05$). (C) Micrographs showing multiple views of lung tissue harvested from mice treated with bleomycin for 3 weeks. The tissues were double stained with B-CHP and an anti-MMP2 antibody, which were visualized using AlexaFluor647-labeled streptavidin and AlexaFluor555-labeled donkey anti-rabbit IgG H&L, respectively. Yellow arrows mark the locations where high MMP2 signals overlap with decreased CHP signals. Additional examples are provided in Figure S7. Scale bars: 200 μm (A), 50 μm (C).

indicated by the highly localized, bright F-CHP deposits appearing in samples beginning 1 week after bleomycin treatment (Figure 5A). Representative images of F-CHP staining and quantitative analysis demonstrated that (i) the number of “bright spots” was significantly higher in the subpleural area of the lungs relative to the center, particularly after week 3, and that (ii) the overall CHP signals in both the central and subpleural areas increased as the disease progressed from week 1 to week 3 and persisted through week 4 (Figure 5, A and B). These spatial and temporal schemes are in strong

agreement with a recent study demonstrating that the inflammation and fibrosis observed in this mouse model are limited to the subpleural portion of the lung.⁴⁸ Co-staining of the tissues with B-CHP and an anti-MMP2 antibody showed that MMP2 expression followed a spatial and temporal pattern similar to that observed with the CHP signals (Figure S6). In magnified images of the costained fields, we noted that areas displaying high MMP2 signals often overlapped with zones of decreased CHP intensity (Figure 5C, arrows; Figure S7), perhaps presenting a snapshot of the MMP2-dependent

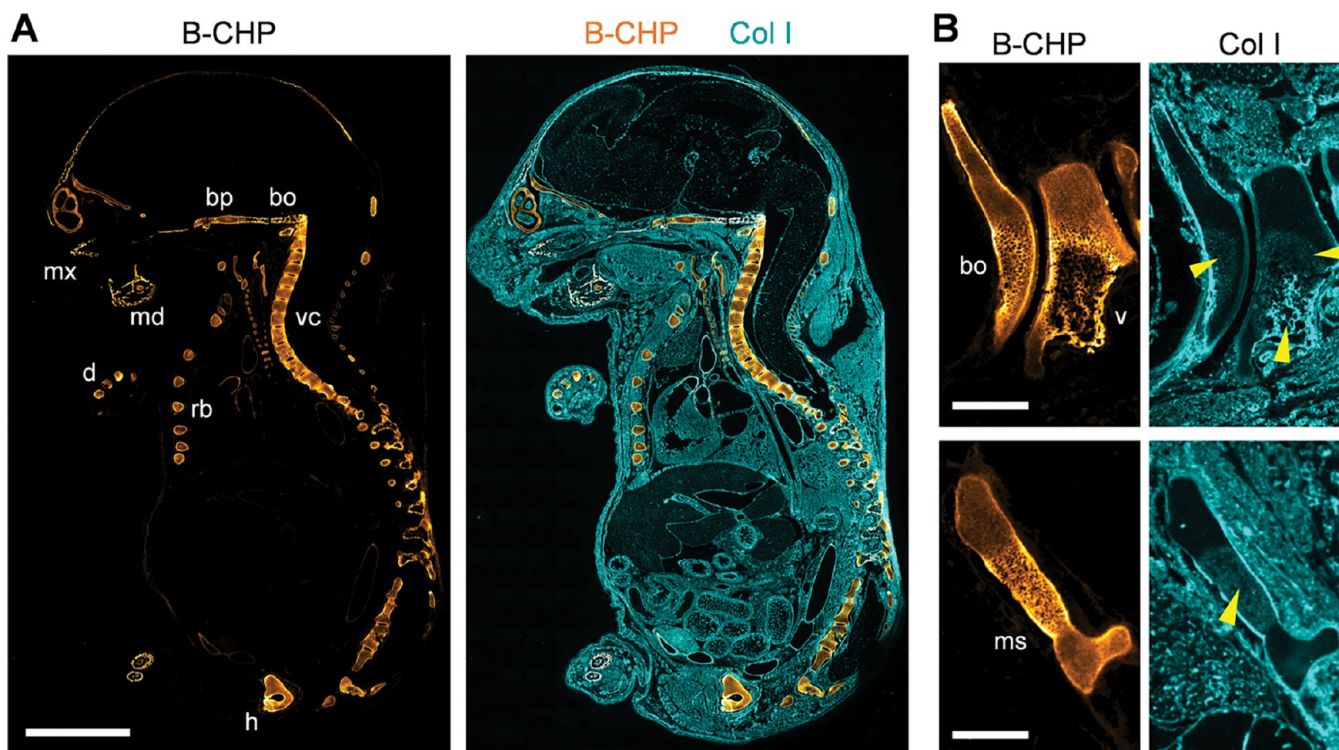


Figure 6. Endochondral ossification. (A) Localization of CHP binding in a sagittal section of an 18 d.p.c. mouse embryo (E18) double stained with B-CHP (detected by AlexaFluor647-streptavidin, orange) and an anti-collagen I antibody (detected by AlexaFluor555-labeled donkey anti-rabbit IgG H&L, cyan). *mx*, maxilla; *md*, mandibular bone; *bp*, basisphenoid bone; *bo*, basioccipital bone; *vc*, vertebral column; *rb*, rib; *h*, hipbone; *d*, digital bones. (B) Magnified views of the basioccipital bone (*bo*) beside the C1 vertebra (*v*) (top images) and the manubrium sterni (*ms*, bottom images) in the sagittal section of a 17 d.p.c. mouse embryo (E17) stained in the same fashion. High levels of CHP binding are found in the hypertrophic zone surrounding the newly deposited collagen I bone matrix (yellow arrow heads), which is visualized by the anti-collagen I antibody. Scale bars: 3 mm (A), 0.5 mm (B).

digestion of denatured collagen chains within the lung ECM.^{49–51} To the best of our knowledge, our CHP staining results provide the first direct evidence of the structural abnormality of collagen molecules within fibrotic tissues (Figures 4 and 5).

Bone Development. In mammals, most bone is formed by endochondral ossification, a process wherein a cartilage template is eventually degraded by hypertrophic chondrocytes and osteoblast-like cells and then replaced by mineralized bone tissue.⁵² Given a collagen remodeling program highlighted by the proteolytic replacement of type II and X collagen by newly formed type I collagen,⁵² we sought to visualize this classic developmental process in mouse embryo sagittal sections by CHP staining (Figure 6). In contrast to type I collagen staining that highlighted the uniform distribution of collagen in the 18-day postcoitum embryo (designated as E18), collagen degradation detected by CHP was localized exclusively in the developing skeletal tissue, including the mandibular bone, maxilla, basioccipital and basisphenoid bone, vertebrae, ribs, hipbone, and digital bones (Figure 6A). No CHP binding was detected in nonskeletal tissues, such as skin, kidney, muscle, or heart. This distinct spatial pattern closely matches previous studies using *in situ* hybridization techniques demonstrating that interstitial collagenase expression is restricted to skeletal tissue during mouse embryogenesis.^{53,54} Magnified images further revealed that CHP signals were particularly high in the hypertrophic cartilage zone abutting ossification sites (Figure 6B), supporting the conclusion that the collagen-degrading activity of hypertrophic chondrocytes resides in this zone. CHP

staining of a series of embryos from E12 to E18 demonstrated that ossification-zone-associated collagen degradation could be clearly detected after E14 (Figure S8), a finding in agreement with previous studies showing that the expression of interstitial collagenase begins on day 15 of gestation,⁵⁵ whereas the major collagenase expressed at ossification sites (*i.e.*, MMP13) is detectable from E14.5.⁵⁶ Taken together, our data indicate that CHP binding can be used to follow spatiotemporal changes in collagen remodeling during endochondral ossification and skeletal development.

Skin Aging. In chronologically aged skin, structural changes in the type I collagen-rich dermis have been linked to increased MMP expression^{22,29,57} and, presumably, collagenolytic activity. To determine whether degraded collagen fragments can be detected in aging tissues, we stained skin samples obtained from sun-protected 21-day-old *versus* 9-month-old mice with B-CHP followed by AlexaFluor647-streptavidin. Fluorescence micrographs revealed that higher levels of degraded collagen fragments were clearly present in the dermis of the aged skin samples (Figure 7A). We also conducted SHG microscopy to visualize the collagen fibers²⁰ in conjunction with fluorescence microscopy. The F-CHP-stained skin samples were imaged using multiphoton confocal microscopy, simultaneously acquiring the collagen fiber SHG signal and the F-CHP fluorescence signal on separate channels. SHG imaging revealed that mature collagen fibers were observable only in the old skin samples (Figure 7B), presumably because the collagen fibers in the young skin were not sufficiently sized or organized to generate a detectable signal. Meanwhile, the F-CHP signal clearly

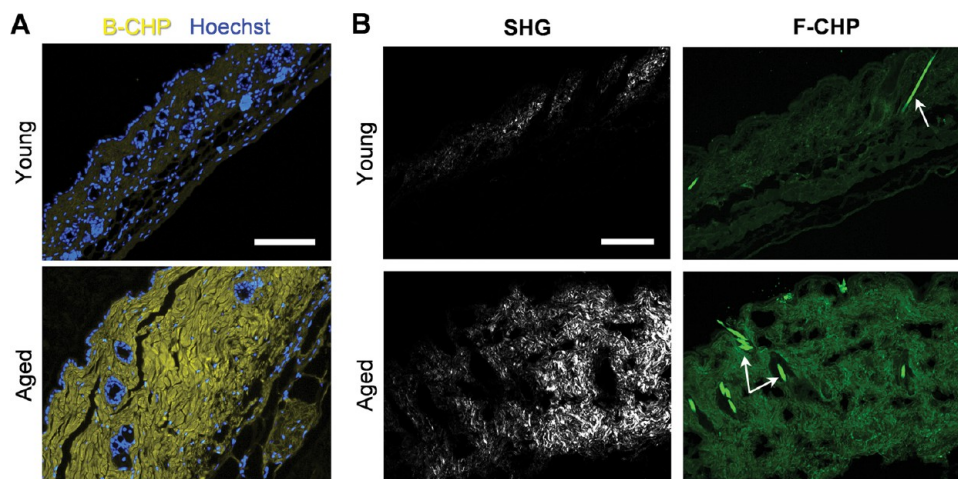


Figure 7. Chronological skin aging. (A) Representative fluorescence micrographs of formalin-fixed paraffin-embedded skin sections from 21-day (young) versus 9-month-old mice (aged), stained with Hoechst 33342 (blue) and B-CHP (detected by AlexaFluor647-streptavidin, yellow). (B) Representative views from simultaneous multiphoton imaging of frozen skin sections from the same group of mice, stained by F-CHP, showing the distinct fiber morphologies (via SHG, white) and degraded collagen content (via F-CHP, green). Remaining hair shafts (white arrows) are strongly autofluorescent. Both experiments were performed on skin samples obtained from 3 mice at each age with similar results. Scale bars: 100 μm (A), 150 μm (B).

separated the two groups (Figure 7B). This suggests that collagen in young skin is intact at the molecular level, but immature in terms of fiber formation, whereas collagen in aged skin has a mature fiber structure, but with partial degradation and denaturation. These results highlight the fact that the two techniques depict distinct aspects of the dermal architecture; that is, while SHG imaging integrates the general collagen-fiber morphology, the CHP stain specifically targets the damaged collagen molecules.

In this study, we demonstrated that denatured collagen generated during tissue remodeling can be effectively detected using CHP hybridization in a variety of tissues in pathologic as well as developmental states. The spatiotemporal features of collagen degradation as detected by CHP staining in diseased or developing tissues correlated closely with the time course of MMP expression and activity, as well as the distribution of MMPs reported by others in similar animal models.^{37,38,48,53,54} Furthermore, CHP staining without the heat-dissociation step confirmed the absence of signals in tissues that were stained with the folded CHP trimers (Figure S9), verifying that the CHP binding visualized in all the images is driven by the triple-helical hybridization and is not due to nonspecific interactions and autofluorescence of the tissues. CHP is designed to target the dominant secondary protein structure of the entire collagen family. As a result, the peptide has the ability to bind multiple, if not all, types of denatured collagen. In agreement with an in-gel Western blot analysis in our previous study,⁵⁸ our data here indicate that CHP binds to denatured collagens in cartilage (type II), kidney (type IV), lung and skin (type I, III) as well as those from different species (i.e., mouse, rat, porcine, and human). We also note that CHP specifically detects degraded collagen without antigen retrieval in formalin-fixed, paraffin-embedded (FFPE) sections, a processing protocol that proves problematic for antibodies whose epitopes can be modified during sample preparation. Thus, CHP should be considered a broad-spectrum reagent for detecting collagen degradation. However, it should be noted that its broad-spectrum affinity limits its ability to distinguish between different degraded collagen types, a shortcoming that could be overcome when

CHP staining is used in conjunction with type-specific collagen antibodies. We also note that several noncollagenous proteins,²⁶ such as complement factor C1q, mannose binding protein, and bacterial collagen-like proteins, also contain short triple-helical domains of Gly-X-Y repeats and that after unfolding they could be targets for CHP hybridization.⁵⁸ However, it critically depends on whether their collagen-like triple helices are susceptible to enzymatic digestion and unfolding *in vivo*,^{59,60} a question that remains to be fully investigated. In addition, we do not recommend CHP staining on FFPE samples processed with common antigen retrieval methods, such as microwaving with citric acid or proteinase K, which might denature collagen molecules and enhance CHP binding artificially.

Currently, attempts to assess collagen degradation (whether *in vivo* or *in vitro*) are indirect and alternatively focus on the detection of collagenolytic proteinases (e.g., MMP-1, MMP-8, MMP-13, MMP-14, cathepsin K). While mRNA levels for collagenolytic enzymes can be monitored by the reverse transcription polymerase chain reaction (RT-PCR) and protein expression *via* Western blotting or enzyme-linked immunosorbent assays (ELISA), the precise identity of the proteinases involved in collagenolysis cannot be determined, as the enzymes are expressed as inactive zymogens. Furthermore, even following activation, collagenolytic enzymes can be inhibited by endogenous inhibitors (e.g., TIMPs, cystatin, alpha-2-macroglobulin),³ which are often jointly upregulated.⁴⁶ *In situ* zymography is a method used frequently to detect and localize MMP activities in frozen tissues using fluorescently labeled gelatin or collagen as a substrate.⁶¹ However, the technique is more sensitive for detecting gelatinases as opposed to true collagenases and does not assess the structural integrity of the surrounding ECM. On the contrary, the CHP stain provides direct evidence of collagen degradation, albeit without identifying the responsible collagenases. In cases where the integrity of the ECM is critical for the pathologic outcome, such as in cancer cell metastasis or atherosclerotic plaque rupture, interrogating the structural status of the collagen matrix directly may be more informative than the identity of the involved

proteinase(s). In addition, if used in tandem with more standard collagenase detection methods, CHP could be a tool to validate, or even contradict, the links existing within the complex interaction network of collagenases and ECM *in vivo*.

CONCLUSIONS

As outlined in this study, degraded collagen is an informative marker of tissue damage and remodeling whose level reflects the progression of disease as well as the regulation of developmental programs. Conventional histology stains often require a trained pathologist for interpretation, and the changes in the tissue structure are difficult to quantify. By contrast, the CHP stain provides a straightforward method to visualize and quantify tissue remodeling *in situ*. From the practical aspect, as CHP is not an antibody-based approach, there are no species conflicts between CHP and a tissue sample or between CHP and a primary antibody used during double staining. With these advantages, the CHP probe can be used as a preferred special stain to analyze animal tissue or human biopsy with diverse biological and medical applications, including phenotyping in developmental biology, disease staging and prognosis, and therapeutic screening. Interestingly, CHP is highly stable in serum⁶² and possesses a chemically inert sequence that can be readily conjugated to an imaging probe or a therapeutic agent. We previously demonstrated CHP's ability to target pathologic tissues *in vivo*²⁴ and the ease to prepare CHP-functionalized nanomaterials.^{34,63} With the results of this study, we propose that CHP could be further developed into a useful agent for *in vivo* imaging and drug delivery.

METHODS

Reagents. AlexaFluor555-donkey-anti-rabbit (ab150074), rabbit anti-MMP-2 antibody (ab37150), anti-collagen I antibody (ab34710), and Fluoroshield (ab104135) were obtained from Abcam. The anti-CD68 antibody (MCA1957T) and goat-F(ab')₂-anti-rat IgG:FITC (STAR69) were acquired from BIO-RAD. The anti-collagen IV (rabbit) antibody (600-401-106-0.1) was obtained from Rockland. Goat serum (G90023), bovine serum albumin (BSA, A9647), xylenes, ethyl alcohol, and all other chemicals were obtained from Sigma-Aldrich. The endogenous biotin-blocking kit (E21390), the neutravidin-horseradish peroxidase conjugate (A2665), Alexa-Fluor647-streptavidin conjugate (S21374), and Hoechst 33342 (R37605) were obtained from Thermo Fisher Scientific. DAB substrate kit (SK-4100) and hematoxylin QS (H3404) were obtained from Vector Laboratories.

The 5-FAM and biotin CHP peptides were obtained from 3Helix Inc. The peptides [F-CHP, sequence: 5-FAM-GGG-(GPO)₉, GGG: spacer; B-CHP, sequence: biotin-Ahx-(GPO)₉, Ahx: aminohexanoic acid] were synthesized using the standard solid phase peptide synthesis technique and purified using reverse phase high-performance liquid chromatography according to previous reports.^{24,58,64} The molecular weights of the purified peptides were verified using matrix-assisted laser desorption/ionization time-of-flight (MALDI-TOF) MS on a Bruker UltrafleXtreme. The lyophilized, purified peptide powders were dissolved in deionized water at a concentration of 100 μ M and stored at 4 °C.

Tissue Samples and Animals. Porcine medial cruciate ligaments were a kind gift from the Jeffrey Weiss group (University of Utah). Frozen human cartilage tissue sections from a 73-year-old OA patient were purchased from OriGene (catalog numbers: CS522857 and CS522859). A panel of the C57 mouse embryo sagittal frozen tissue sections was obtained from Zyagen (MF-104-008-C57). Frozen, hair-removed skin tissues from the lower back of 3-week-old and 9-month-old male C57BL/6 mice were purchased from Charles River Laboratories. Two pieces of tissue were dissected from each skin sample. One piece was snap-frozen in optimal cutting temperature

(OCT) compound, and the other piece was fixed in formalin followed by paraffin embedding; both were cut into 5 μ m thick sections. Infarcted hearts from 8-week-old C57BL/6J mice were purchased from CL Laboratory (Baltimore, MD, USA). Hearts were harvested from mice at varying time points (three mice per group) after a standard left anterior descending artery occlusion procedure.³⁷ Each heart was axially dissected into two halves. The bottom half was snap-frozen in OCT, and the top half was fixed in formalin followed by paraffin embedding; 10 μ m thick sections exposing the whole axial plane of the hearts were cut from the OCT- and paraffin-embedded tissue blocks.

The following study procedure was approved by the University of Utah Institutional Animal Care and Use Committee. Glomerulonephritis was induced by tail vein injection of the monoclonal anti-Thy-1 Ab OX-7 (1.75 mg/kg body weight) to a male rat (220 to 250 g in body weight) on day 0. The OX-7 mAb binds to a Thy-1 epitope on the surface of mesangial cells and causes complement-dependent cell lysis followed by exuberant matrix synthesis and deposition.⁴¹ Normal control animals were injected with the same volume of phosphate-buffered saline (PBS). The experiment was performed using three rats per group. At day 12, the rats were anesthetized with isoflurane, and the kidneys perfused with 30 mL of cold PBS and harvested. One piece of renal cortical tissue from individual rats was snap-frozen, and one piece of renal cortical tissue was fixed in 10% neutralized formalin and embedded in paraffin for histological staining as described previously.⁴¹

The following study procedure was approved by the Institutional Animal Care and Use Committee of MedImmune LLC. Lung fibrosis in C57BL/6 mice (female, 10-week-old; Jackson Laboratories) was induced with bleomycin at a dose of 70 mg/kg *via* osmotic minipumps (ALZED 1007D) designed to deliver 0.5 μ L/h for 7 days. On day 0, the osmotic minipumps, containing either 100 μ L of saline vehicle or bleomycin, were implanted under isoflurane anesthesia under the skin on the back of the mice posterior to the scapulae. Mice were euthanized at indicated times, and the lungs were inflated with 1 mL of 50% OCT in PBS. The right lung lobes were harvested, snap-frozen in OCT, and cut into 5 μ m thick sections.

Tissue sectioning and the PAS staining using paraffin-embedded kidney tissue were performed at the University of Utah health care research histology core facility using standard procedures.

CHP Staining. For OCT-embedded tissue sections, the OCT compound was removed by rinsing with PBS for 5 min after tissue slides were warmed to room temperature. For FFPE tissue sections, paraffin was removed by rinsing with xylene, 100% ethanol, 95% ethanol, 50% ethanol, and deionized water for two 5 min cycles of each solvent in consecutive order. The deparaffinized tissue was directly used for staining without any antigen-retrieval process. After the embedding material was removed, 5% goat serum in PBS was added to the tissue sections and incubated for 20 min at room temperature to block nonspecific binding. For B-CHP staining, any endogenous biotin in the tissue was blocked using the endogenous biotin-blocking kit following the manufacturer's protocol after the serum blocking step. Because CHP can self-assemble into homotrimers in solution over time (*e.g.*, during storage at 4 °C) and lose its driving force for collagen hybridization, the trimeric CHP was thermally dissociated to single strands by heating briefly at 80 °C before it was used to bind unfolded collagen.²⁵ To prevent undesired thermal denaturation of the tissue, the 80 °C CHP solution was quenched quickly to room temperature immediately prior to addition to tissue samples (dead time <2 min). The CHP trimerization has a third-order folding rate with a half-time on the order of hours at low μ M concentrations.^{26,65,66} Therefore, the heating and quenching protocol used here (Figure S1) ensures that CHP strands predominate in the active monomer form until exposed to denatured collagen. After the blocking solutions were gently removed from the slides, heat-activated solutions of single-strand CHPs were added to the tissue sections in the following fashion. CHP solution (15 μ M of B-CHP or F-CHP, 50–200 μ L per section) in PBS or PBS containing 1% BSA (when costaining with an antibody) was heated for 5 min in an 80 °C water bath to dissociate the trimeric peptides, followed by immediate incubation in an ice/water bath (for

15–90 s depending on the solution volume) to quench the hot solution to room temperature. When needed, an antibody was diluted into this quenched CHP solution for costaining. The solution containing the quenched CHP monomers was quickly pipetted to each slide (usually 50–200 μL per section) within 1 min. The tissue samples were incubated in a humidity chamber at 4 $^{\circ}\text{C}$ overnight. After staining, the slides were incubated for 5 min in 100 mL of PBS at room temperature to remove the unbound material and the washing step was repeated three times. For B-CHP staining, the tissue sections were subsequently incubated with AlexaFluor647-labeled streptavidin (0.005 mg/mL) in a PBS solution containing 1% BSA. To detect the costained primary antibody, a labeled secondary antibody was either diluted into the AlexaFluor647-streptavidin solution (for B-CHP costaining) or added to the slides directly after dilution in a PBS solution containing 1% BSA (for F-CHP costaining). The tissues were incubated with the streptavidin and/or secondary antibody solution in a humidity chamber for 1 h at room temperature. Where indicated, cell nuclei were stained with Hoechst 33342 in PBS for 20 min according to the manufacturer's recommendation. Finally, the tissue sections were rinsed with PBS three times and mounted with Fluoroshield. The specific CHP, antibody types, and concentrations used in each experiment are presented in Table S1. All histological staining experiments were performed on at least three different sections from each tissue sample. For the myocardial infarction, glomerulonephritis, lung fibrosis, and skin aging experiments, tissue samples from three animals within each experimental group (e.g., the normal control group, the week 3 group) were analyzed.

Fluorescence Microscopy and Image Analysis. All tissue sections in this work were imaged or scanned using an EVOS FL auto cell imaging system (Thermo Fisher Scientific) using 4, 10, 20, or 40 \times objective lens. Fluorescence from Hoechst 33342, 5-FAM/FITC, AlexaFluor555, and AlexaFluor647 was detected using the DAPI, GFP, RFP, and Cy5 light cube, respectively. The tissues stained by hematoxylin and HRP-neutravidin were imaged under a bright-light field. Large whole-section images were created through view-to-view scanning and image-stitching automatically performed by the EVOS imaging system. Identical microscopic settings were used to allow direct comparison of CHP or antibody binding among the samples within each experiment.

For clarity, images were assigned with pseudocolors using the LUT color schemes available in the ImageJ software with heat-map-like multicolor schemes selected for images in Figures 3A, 5A, and 5C to highlight the intensity variation. Fluorescence signals resulting from B-CHP binding to the heart sections in the myocardial infarction experiment were analyzed in the ImageJ software using measurements of the mean intensity times the area of all remaining pixels after background subtraction. The CHP signals were normalized by the size of each heart section (estimated by the total area of all positive pixels in the images of the Hoechst 33342 stain) and are shown in Figure 3B. F-CHP fluorescence from fibrotic lung tissues was analyzed in the ImageJ software using measurements of the mean intensity times the area of all remaining pixels after background subtraction. Two photomicrographs of the central area and three photomicrographs of the subpleural areas taken from each lung section were analyzed, and the procedure was repeated for three lung samples in each experimental group. The quantified values were averaged in each category and are presented in Figure 5B.

SHG Imaging. A drop of PBS was applied to each of the frozen mouse skin section previously stained with F-CHP (three per age group) and covered with a glass cover slide. The slides were immersed in deionized water and imaged by a custom Prairie View Ultima multiphoton microscope (Bruker). A single excitation wavelength at 800 nm was used to simultaneously visualize collagen fibers and F-CHP binding in the tissue. The resulting SHG and 5-FAM fluorescence signals were detected at 435–485 nm and 500–550 nm, respectively. Z-stack images were acquired for the entire 5 μm section depth and stacked into a single image using the ImageJ software.

Statistics. The quantitative results are presented as the mean + standard error. Comparisons among groups were performed using

one-way ANOVA with *post hoc* Tukey HSD test. Differences were considered statistically significant at $P < 0.05$.

ASSOCIATED CONTENT

Supporting Information

The Supporting Information is available free of charge on the ACS Publications website at DOI: 10.1021/acsnano.7b03150.

Additional microscopic fluorescence imaging results, near-infrared fluorescence images of MMP activity in bleomycin-treated mice, and specific protocol steps for antibody and CHP staining (PDF)

AUTHOR INFORMATION

Corresponding Author

*Phone: 801.587.0215. E-mail: yang.d.li@utah.edu.

ORCID

Jeongmin Hwang: 0000-0001-8799-3209

S. Michael Yu: 0000-0002-5171-2644

Yang Li: 0000-0003-4729-7860

Author Contributions

J.H., Y.H., T.J.B., N.C.P., and Y.L. designed the study and performed the experiments, and J.H., Y.H., T.J.B., N.C.P., J.C., S.J.W., S.M.Y., and Y.L. analyzed the results and discussed the implications. All authors contributed to writing and editing of the manuscript.

Notes

The authors declare the following competing financial interest(s): Y.L. and S.M.Y. are founders and shareholders of 3Helix Inc, which commercializes the collagen hybridizing peptides.

ACKNOWLEDGMENTS

This work was supported by the National Institutes of Health (ORIP, R43OD021986) awarded to Y.L. We thank the National Institutes of Health and the Department of Defense (NIH, R01AR060484, R21AR065124, and DOD W81XWH-12-1-0555 awarded to S.M.Y.) for supporting the research of the CHP technology.

REFERENCES

- Brinckmann, J. Collagens at a Glance. In *Collagen: Primer in Structure, Processing and Assembly*; Brinckmann, J.; Notbohm, H.; Müller, P. K., Eds.; Springer: Berlin, Heidelberg, 2005; pp 1–6.
- Shoulders, M. D.; Raines, R. T. Collagen Structure and Stability. *Annu. Rev. Biochem.* **2009**, *78*, 929–958.
- Bonnans, C.; Chou, J.; Werb, Z. Remodelling the Extracellular Matrix in Development and Disease. *Nat. Rev. Mol. Cell Biol.* **2014**, *15*, 786–801.
- Page-McCaw, A.; Ewald, A. J.; Werb, Z. Matrix Metalloproteinases and the Regulation of Tissue Remodelling. *Nat. Rev. Mol. Cell Biol.* **2007**, *8*, 221–233.
- Wahyudi, H.; Reynolds, A. A.; Li, Y.; Owen, S. C.; Yu, S. M. Targeting Collagen for Diagnostic Imaging and Therapeutic Delivery. *J. Controlled Release* **2016**, *240*, 323–331.
- Tlsty, T. D.; Coussens, L. M. Tumor Stroma and Regulation of Cancer Development. *Annu. Rev. Pathol.: Mech. Dis.* **2006**, *1*, 119–150.
- Liotta, L. A.; Kohn, E. C. The Microenvironment of the Tumour-Host Interface. *Nature* **2001**, *411*, 375–379.
- Seandel, M.; Noack-Kunmann, K.; Zhu, D.; Aimes, R. T.; Quigley, J. P. Growth Factor-Induced Angiogenesis *In Vivo* Requires Specific Cleavage of Fibrillar Type I Collagen. *Blood* **2001**, *97*, 2323–2332.

- (9) Finn, A. V.; Nakano, M.; Narula, J.; Kolodgie, F. D.; Virmani, R. Concept of Vulnerable/Unstable Plaque. *Arterioscler., Thromb., Vasc. Biol.* **2010**, *30*, 1282–1292.
- (10) Troeberg, L.; Nagase, H. Proteases Involved in Cartilage Matrix Degradation in Osteoarthritis. *Biochim. Biophys. Acta, Proteins Proteomics* **2012**, *1824*, 133–145.
- (11) Dejica, V. M.; Mort, J. S.; Laverty, S.; Percival, M. D.; Antoniou, J.; Zukor, D. J.; Poole, A. R. Cleavage of Type II Collagen by Cathepsin K in Human Osteoarthritic Cartilage. *Am. J. Pathol.* **2008**, *173*, 161–169.
- (12) Nielsen, L. F.; Moe, D.; Kirkeby, S.; Garbarsch, C. Sirius Red and Acid Fuchsin Staining Mechanisms. *Biotech. Histochem.* **1998**, *73*, 71–77.
- (13) Dayan, D.; Hiss, Y.; Hirshberg, A.; Bubis, J. J.; Wolman, M. Are the Polarization Colors of Picrosirius Red-Stained Collagen Determined Only by the Diameter of the Fibers? *Histochemistry* **1989**, *93*, 27–29.
- (14) Fledelius, C.; Johnsen, A. H.; Cloos, P. A. C.; Bonde, M.; Qvist, P. Characterization of Urinary Degradation Products Derived from Type I Collagen: Identification of a B-Isomerized Asp-Gly Sequence within the C-Terminal Telopeptide (A1) Region. *J. Biol. Chem.* **1997**, *272*, 9755–9763.
- (15) Lohmander, L. S.; Atley, L. M.; Pietka, T. A.; Eyre, D. R. The Release of Crosslinked Peptides from Type II Collagen into Human Synovial Fluid Is Increased Soon after Joint Injury and in Osteoarthritis. *Arthritis Rheum.* **2003**, *48*, 3130–3139.
- (16) Sand, J. M.; Larsen, L.; Hogaboam, C.; Martinez, F.; Han, M.; Røssel Larsen, M.; Nawrocki, A.; Zheng, Q.; Asser Karsdal, M.; Leeming, D. J. MMP Mediated Degradation of Type IV Collagen Alpha 1 and Alpha 3 Chains Reflects Basement Membrane Remodeling in Experimental and Clinical Fibrosis – Validation of Two Novel Biomarker Assays. *PLoS One* **2013**, *8*, e84934.
- (17) Billingham, R. C.; Dahlberg, L.; Ionescu, M.; Reiner, A.; Bourne, R.; Rorabeck, C.; Mitchell, P.; Hambor, J.; Diekmann, O.; Tschesche, H.; Chen, J.; Van Wart, H.; Poole, A. R. Enhanced Cleavage of Type II Collagen by Collagenases in Osteoarthritic Articular Cartilage. *J. Clin. Invest.* **1997**, *99*, 1534–1545.
- (18) Croucher, L. J.; Hollander, A. P. Differential Detection of Type II Collagen N-Terminal and C-Terminal Denaturation Epitopes in Degrading Cartilage. *Mol. Pathol.* **1999**, *52*, 323–331.
- (19) Xu, J.; Rodriguez, D.; Petittler, E.; Kim, J. J.; Hangai, M.; Yuen, S. M.; Davis, G. E.; Brooks, P. C. Proteolytic Exposure of a Cryptic Site within Collagen Type IV Is Required for Angiogenesis and Tumor Growth *In Vivo*. *J. Cell Biol.* **2001**, *154*, 1069–1079.
- (20) Chen, X.; Nadiarynkh, O.; Plotnikov, S.; Campagnola, P. J. Second Harmonic Generation Microscopy for Quantitative Analysis of Collagen Fibrillar Structure. *Nat. Protoc.* **2012**, *7*, 654–669.
- (21) Matteini, P.; Cicchi, R.; Ratto, F.; Kapsokalyvas, D.; Rossi, F.; de Angelis, M.; Pavone, Francesco, S.; Pini, R. Thermal Transitions of Fibrillar Collagen Unveiled by Second-Harmonic Generation Microscopy of Corneal Stroma. *Biophys. J.* **2012**, *103*, 1179–1187.
- (22) Fligel, S. E. G.; Varani, J.; Datta, S. C.; Kang, S.; Fisher, G. J.; Voorhees, J. J. Collagen Degradation in Aged/Photodamaged Skin *In Vivo* and after Exposure to Matrix Metalloproteinase-1 *In Vitro*. *J. Invest. Dermatol.* **2003**, *120*, 842–848.
- (23) Kadler, K. E.; Holmes, D. F.; Trotter, J. A.; Chapman, J. A. Collagen Fibril Formation. *Biochem. J.* **1996**, *316*, 1–11.
- (24) Li, Y.; Foss, C. A.; Summerfield, D. D.; Doyle, J. J.; Torok, C. M.; Dietz, H. C.; Pomper, M. G.; Yu, S. M. Targeting Collagen Strands by Photo-Triggered Triple-Helix Hybridization. *Proc. Natl. Acad. Sci. U. S. A.* **2012**, *109*, 14767–14772.
- (25) Li, Y.; Yu, S. M. Targeting and Mimicking Collagens *via* Triple Helical Peptide Assembly. *Curr. Opin. Chem. Biol.* **2013**, *17*, 968–975.
- (26) Engel, J.; Bächinger, H. P. Structure, Stability and Folding of the Collagen Triple Helix. In *Collagen*; Brinckmann, J.; Notbohm, H.; Müller, P. K., Eds.; Springer Verlag: Berlin, Heidelberg, 2005; Vol. 247, pp 7–33.
- (27) Danielsen, C. C. Thermal Stability of Human-Fibroblast-Collagenase-Cleavage Products of Type-I and Type-III Collagens. *Biochem. J.* **1987**, *247*, 725–729.
- (28) Chung, L.; Dinakarpanian, D.; Yoshida, N.; Lauer-Fields, J. L.; Fields, G. B.; Visse, R.; Nagase, H. Collagenase Unwinds Triple-Helical Collagen Prior to Peptide Bond Hydrolysis. *EMBO J.* **2004**, *23*, 3020–3030.
- (29) Fisher, G. J.; Kang, S.; Varani, J.; Bata-Csorgo, Z.; Wan, Y.; Datta, S.; Voorhees, J. J. Mechanisms of Photoaging and Chronological Skin Aging. *Arch. Dermatol.* **2002**, *138*, 1462–1470.
- (30) Li, Y.; Foss, C. A.; Pomper, M. G.; Yu, S. M. Imaging Denatured Collagen Strands *In Vivo* and *Ex Vivo* *via* Photo-Triggered Hybridization of Caged Collagen Mimetic Peptides. *J. Visualized Exp.* **2014**, e51052.
- (31) Li, Y.; San, B. H.; Kessler, J. L.; Kim, J. H.; Xu, Q.; Hanes, J.; Yu, S. M. Non-Covalent Photo-Patterning of Gelatin Matrices Using Caged Collagen Mimetic Peptides. *Macromol. Biosci.* **2015**, *15*, 52–62.
- (32) Persikov, A. V.; Ramshaw, J. A. M.; Kirkpatrick, A.; Brodsky, B. Amino Acid Propensities for the Collagen Triple-Helix. *Biochemistry* **2000**, *39*, 14960–14967.
- (33) Yu, S. M.; Li, Y.; Kim, D. Collagen Mimetic Peptides: Progress Towards Functional Applications. *Soft Matter* **2011**, *7*, 7927–7938.
- (34) Santos, J. L.; Li, Y.; Culver, H. R.; Yu, M. S.; Herrera-Alonso, M. Conducting Polymer Nanoparticles Decorated with Collagen Mimetic Peptides for Collagen Targeting. *Chem. Commun.* **2014**, *50*, 15045–15048.
- (35) Pritzker, K. P. H.; Gay, S.; Jimenez, S. A.; Ostergaard, K.; Pelletier, J. P.; Revell, P. A.; Salter, D.; van den Berg, W. B. Osteoarthritis Cartilage Histopathology: Grading and Staging. *Osteoarthritis Cartilage* **2006**, *14*, 13–29.
- (36) Weinberger, T.; Schulz, C. Myocardial Infarction: A Critical Role of Macrophages in Cardiac Remodeling. *Front. Physiol.* **2015**, *6*, 10.3389/fphys.2015.00107
- (37) Nguyen, J.; Sievers, R.; Motion, J. P. M.; Kivimäe, S.; Fang, Q.; Lee, R. J. Delivery of Lipid Micelles into Infarcted Myocardium Using a Lipid-Linked Matrix Metalloproteinase Targeting Peptide. *Mol. Pharmaceutics* **2015**, *12*, 1150–1157.
- (38) Chen, J.; Tung, C.-H.; Allport, J. R.; Chen, S.; Weissleder, R.; Huang, P. L. Near-Infrared Fluorescent Imaging of Matrix Metalloproteinase Activity after Myocardial Infarction. *Circulation* **2005**, *111*, 1800–1805.
- (39) Lenz, O.; Elliot, S. J.; Stetler-Stevenson, W. G. Matrix Metalloproteinases in Renal Development and Disease. *J. Am. Soc. Nephrol.* **2000**, *11*, 574–581.
- (40) Floege, J.; Johnson, R. J.; Gordon, K.; Iida, H.; Pritzl, P.; Yoshimura, A.; Campbell, C.; Alpers, C. E.; Couser, W. G. Increased Synthesis of Extracellular Matrix in Mesangial Proliferative Nephritis. *Kidney Int.* **1991**, *40*, 477–488.
- (41) Huang, Y.; Haraguchi, M.; Lawrence, D. A.; Border, W. A.; Yu, L.; Noble, N. A. A Mutant, Noninhibitory Plasminogen Activator Inhibitor Type 1 Decreases Matrix Accumulation in Experimental Glomerulonephritis. *J. Clin. Invest.* **2003**, *112*, 379–388.
- (42) Lovett, D. H.; Johnson, R. J.; Marti, H. P.; Martin, J.; Davies, M.; Couser, W. G. Structural Characterization of the Mesangial Cell Type IV Collagenase and Enhanced Expression in a Model of Immune Complex-Mediated Glomerulonephritis. *Am. J. Pathol.* **1992**, *141*, 85–98.
- (43) Steinmann-Niggli, K.; Ziswiler, R.; Küng, M.; Marti, H. P. Inhibition of Matrix Metalloproteinases Attenuates Anti-Thy1.1 Nephritis. *J. Am. Soc. Nephrol.* **1998**, *9*, 397–407.
- (44) Hamano, Y.; Okude, T.; Shirai, R.; Sato, I.; Kimura, R.; Ogawa, M.; Ueda, Y.; Yokosuka, O.; Kalluri, R.; Ueda, S. Lack of Collagen XVIII/Endostatin Exacerbates Immune-Mediated Glomerulonephritis. *J. Am. Soc. Nephrol.* **2010**, *21*, 1445–1455.
- (45) Degryse, A. L.; Tanjore, H.; Xu, X. C.; Polosukhin, V. V.; Jones, B. R.; McMahon, F. B.; Gleaves, L. A.; Blackwell, T. S.; Lawson, W. E. Repetitive Intratracheal Bleomycin Models Several Features of Idiopathic Pulmonary Fibrosis. *Am. J. Physiol. Lung Cell. Mol. Physiol.* **2010**, *299*, L442–452.

- (46) Oggionni, T.; Morbini, P.; Inghilleri, S.; Palladini, G.; Tozzi, R.; Vitulo, P.; Fenoglio, C.; Perlini, S.; Pozzi, E. Time Course of Matrix Metalloproteases and Tissue Inhibitors in Bleomycin-Induced Pulmonary Fibrosis. *Eur. J. Histochem.* **2006**, *50*, 317–325.
- (47) Kim, J. Y.; Choeng, H. C.; Ahn, C.; Cho, S.-H. Early and Late Changes of MMP-2 and MMP-9 in Bleomycin-Induced Pulmonary Fibrosis. *Yonsei Med. J.* **2009**, *50*, 68–77.
- (48) Lee, R.; Reese, C.; Bonner, M.; Tourkina, E.; Hajdu, Z.; Riemer, E. C.; Silver, R. M.; Visconti, R. P.; Hoffman, S. Bleomycin Delivery by Osmotic Minipump: Similarity to Human Scleroderma Interstitial Lung Disease. *Am. J. Physiol. Lung Cell. Mol. Physiol.* **2014**, *306*, L736–748.
- (49) Seltzre, J. L.; Eisen, A. Z. Native Type I Collagen Is Not a Substrate for MMP2 (Gelatinase a). *J. Invest. Dermatol.* **1999**, *112*, 993–994.
- (50) Ohuchi, E.; Imai, K.; Fujii, Y.; Sato, H.; Seiki, M.; Okada, Y. Membrane Type 1 Matrix Metalloproteinase Digests Interstitial Collagens and Other Extracellular Matrix Macromolecules. *J. Biol. Chem.* **1997**, *272*, 2446–2451.
- (51) Pia, V.; Risto, A.-a.; Veli-Matti, K. Matrix Metalloproteinases as Therapeutic Targets in Cancer. *Curr. Cancer Drug Targets* **2005**, *5*, 203–220.
- (52) Ortega, N.; Behonick, D. J.; Werb, Z. Matrix Remodeling During Endochondral Ossification. *Trends Cell Biol.* **2004**, *14*, 86–93.
- (53) Mattot, V.; Raes, M. B.; Henriët, P.; Eeckhout, Y.; Stehelin, D.; Vandenbunder, B.; Desbiens, X. Expression of Interstitial Collagenase Is Restricted to Skeletal Tissue During Mouse Embryogenesis. *J. Cell Sci.* **1995**, *108*, 529–535.
- (54) Gack, S.; Vallon, R.; Schmidt, J.; Grigoriadis, A.; Tuckermann, J.; Schenkel, J.; Weiher, H.; Wagner, E.; Angel, P. Expression of Interstitial Collagenase During Skeletal Development of the Mouse Is Restricted to Osteoblast-Like Cells and Hypertrophic Chondrocytes. *Cell Growth Differ.* **1995**, *6*, 759–767.
- (55) Henriët, P.; Rousseau, G. G.; Eeckhout, Y. Cloning and Sequencing of Mouse Collagenase cDNA Divergence of Mouse and Rat Collagenases from the Other Mammalian Collagenases. *FEBS Lett.* **1992**, *310*, 175–178.
- (56) Tuckermann, J. P.; Pittois, K.; Partridge, N. C.; Merregaert, J.; Angel, P. Collagenase-3 (MMP-13) and Integral Membrane Protein 2a (*Itm2a*) Are Marker Genes of Chondrogenic/Osteoblastic Cells in Bone Formation: Sequential Temporal, and Spatial Expression of *Itm2a*, Alkaline Phosphatase, MMP-13, and Osteocalcin in the Mouse. *J. Bone Miner. Res.* **2000**, *15*, 1257–1265.
- (57) Varani, J.; Warner, R. L.; Gharaee-Kermani, M.; Phan, S. H.; Kang, S.; Chung, J.; Wang, Z.; Datta, S. C.; Fisher, G. J.; Voorhees, J. J. Vitamin A Antagonizes Decreased Cell Growth and Elevated Collagen-Degrading Matrix Metalloproteinases and Stimulates Collagen Accumulation in Naturally Aged Human Skin. *J. Invest. Dermatol.* **2000**, *114*, 480–486.
- (58) Li, Y.; Ho, D.; Meng, H.; Chan, T. R.; An, B.; Yu, H.; Brodsky, B.; Jun, A. S.; Yu, M. S. Direct Detection of Collagenous Proteins by Fluorescently Labeled Collagen Mimetic Peptides. *Bioconjugate Chem.* **2013**, *24*, 9–16.
- (59) Ruiz, S.; Henschen-Edman, A. H.; Nagase, H.; Tenner, A. J. Digestion of C1q Collagen-Like Domain with MMPs-1,-2,-3, and -9 Further Defines the Sequence Involved in the Stimulation of Neutrophil Superoxide Production. *J. Leukocyte Biol.* **1999**, *66*, 416–422.
- (60) Komissarov, A. A.; Declerck, P. J.; Shore, J. D. Mechanisms of Conversion of Plasminogen Activator Inhibitor 1 from a Suicide Inhibitor to a Substrate by Monoclonal Antibodies. *J. Biol. Chem.* **2002**, *277*, 43858–43865.
- (61) Vandooren, J.; Geurts, N.; Martens, E.; Van den Steen, P. E.; Opdenakker, G. Zymography Methods for Visualizing Hydrolytic Enzymes. *Nat. Methods* **2013**, *10*, 211–220.
- (62) Bennink, L. L.; Smith, D. J.; Foss, C. A.; Pomper, M. G.; Li, Y.; Yu, S. M. High Serum Stability of Collagen Hybridizing Peptides. *Mol. Pharmaceutics* **2017**, *14*, 1906–1915.
- (63) San, B. H.; Li, Y.; Tarbet, E. B.; Yu, S. M. Nanoparticle Assembly and Gelatin Binding Mediated by Triple Helical Collagen Mimetic Peptide. *ACS Appl. Mater. Interfaces* **2016**, *8*, 19907–19915.
- (64) Li, Y.; Mo, X.; Kim, D.; Yu, S. M. Template-Tethered Collagen Mimetic Peptides for Studying Heterotrimeric Triple-Helical Interactions. *Biopolymers* **2011**, *95*, 94–104.
- (65) Boudko, S.; Frank, S.; Kammerer, R. A.; Stetefeld, J.; Schulthess, T.; Landwehr, R.; Lustig, A.; Bächinger, H. P.; Engel, J. Nucleation and Propagation of the Collagen Triple Helix in Single-Chain and Trimerized Peptides: Transition from Third to First Order Kinetics. *J. Mol. Biol.* **2002**, *317*, 459–470.
- (66) Ackerman, M. S.; Bhate, M.; Shenoy, N.; Beck, K.; Ramshaw, J. A.; Brodsky, B. Sequence Dependence of the Folding of Collagen-Like Peptides. Single Amino Acids Affect the Rate of Triple-Helix Nucleation. *J. Biol. Chem.* **1999**, *274*, 7668–7673.